Genome-resolved meta-omics ties microbial dynamics to process performance in biotechnology for thiocyanate degradation

Rose S. Kantor,[1] Robert J. Huddy,[2] Ramsunder Iyer,[3,4] Brian C. Thomas,[5] Christopher T. Brown,[1] Karthik Anantharaman,[5] Susannah Tringe,[6] Robert L. Hettich,[3] Susan T. L. Harrison,[2] Jillian F. Banfield[5,7]*

Department of Plant and Microbial Biology, University of California, Berkeley, California, USA[1]; Centre for Bioprocess Engineering Research, Department of Chemical Engineering, University of Cape Town, Cape Town, South Africa[2]; Chemical Sciences Division, Oak Ridge National Laboratory, Oak Ridge Tennessee, USA[3], Graduate School of Genome Science and Technology, University of Tennessee, Knoxville, Tennessee, USA[4]; Department of Earth and Planetary Sciences, University of California, Berkeley, California, USA[5]; Joint Genome Institute, Walnut Creek, California, USA[6]; Department of Environmental Science, Policy, and Management, University of California, Berkeley, California, USA[7]

*Corresponding Author: 307 McCone Hall, University of California, Berkeley, California 94720

ABSTRACT

Remediation of industrial wastewater is important for preventing environmental contamination and enabling water reuse. Biological treatment for one industrial contaminant, thiocyanate (SCN^-), relies upon microbial hydrolysis, but this process is sensitive to high loadings. To examine the activity and stability of a microbial community over increasing SCN^- loadings, we established and operated a continuous-flow bioreactor fed increasing loadings of SCN^-. A second reactor was fed ammonium sulfate to mimic breakdown products of SCN^-. Biomass was sampled from both reactors for metagenomics and metaproteomics, yielding a set of genomes for 144 bacteria and one rotifer that constituted the abundant community in both reactors. We analyzed the metabolic potential and temporal dynamics of these organisms across the increasing loadings. In the SCN^- reactor, *Thiobacillus* strains capable of SCN^- degradation were highly abundant, whereas the ammonium sulfate reactor contained nitrifiers and heterotrophs capable of nitrate reduction. Key organisms in the SCN^- reactor expressed proteins involved in SCN^- degradation, sulfur oxidation, carbon fixation, and nitrogen removal. Lower performance at higher loadings was linked to changes in microbial community composition. This work provides an example of how meta-omics can increase our understanding of industrial wastewater treatment and inform iterative process design and development.

INTRODUCTION

Microbial communities in biotechnology have historically been treated as black boxes, but as molecular methods have improved, our knowledge of these systems has deepened. Increasingly, 'meta-omics' methods are being used to investigate critical processes and potential weak points in biotechnology, such as nitrogen and phosphorus removal or bulking in wastewater treatment.[1-3] In particular, specialized treatment of industrial wastewater has benefited from a genome-resolved meta-omics approach[4-7] using high-throughput sequencing of community genomic DNA (metagenomics) or RNA (metatranscriptomics), or spectral characterization of proteins (metaproteomics). These data can be used to identify the key species involved in processes of interest. Improved understanding of the activities and abundances of these organisms under varying conditions could inform design and operation of these systems.

Thiocyanate (SCN^-) is a widespread industrial contaminant found at especially high concentrations (up to 4000 mg/L) in gold mining effluents. If not remediated, it can affect human health and aquatic organisms.[8-10] Notably, SCN^- is inhibitory toward iron- and sulfur-oxidizing microorganisms used in bio-oxidation processes at some gold mines (such as BIOX®) and therefore must be removed before wastewater can be recycled within a mining site or discharged into the environment. SCN^- can be biodegraded by chemolithoautotrophic bacteria as a source of energy,[11-15] by heterotrophic organisms as a sole source of nitrogen,[16,17] and by complex microbial consortia.[18] The initial degradation products are ammonium, carbon dioxide, and reduced sulfur compounds. An industrial-scale process known as Activated Sludge Tailings Effluent Remediation (ASTER™, Outotec, South Africa) successfully treats SCN-containing wastewater at several gold mines.[19]

Inoculated with sludge from the ASTER™ process, a long-running laboratory-scale SCN-fed bioreactor (known as the "SCN^- stock reactor") at the University of Cape Town contains a characterized, diverse microbial community.[20-22] Previous work on this community implicated several abundant *Thiobacillus* spp. in SCN^- degradation due to the presence of an SCN^- operon in the genomes of these autotrophic bacteria. Results also suggested the potential for nitrogen removal by *Thiobacillus* spp. and other community members, and the presence of heterotrophs.[21] Questions remained regarding community stability at different SCN^- loadings, expression of the observed metabolic potential, and the importance of inter-organism interactions, especially for nitrogen removal. The SCN^- stock reactor provided the inoculum for the bioreactors established in this study.

We used time-series genome-resolved metagenomics, in combination with metaproteomic analyses of the samples from final time point, to track changes in the microbial community of a newly-inoculated SCN^- bioreactor operated with increasing loadings. To enrich for organisms that can use and remove the nitrogen produced by SCN^- degradation, a second reactor with the same inoculum was fed ammonium sulfate ($NH_4(SO_4)_{1/2}$) and molasses but no SCN^-. We describe the microbial community structure, protein expression, and replication rates in both reactors during the experiment. Our analysis linked shifts in community membership to changes in reactor function, highlighted organisms and metabolic pathways active under high-SCN^- conditions, and supported the importance of biofilm in this system.

MATERIALS AND METHODS

Reactor set-up, inoculation, and operation: Two continuous stirred tank reactors (CSTRs) were inoculated with homogenized biofilm and planktonic samples from the long-running SCN^- stock reactor at the University of Cape Town. Reactors were stirred with a pitched-blade impeller at 270 rpm and sparged with filtered air at 900 mL/min. One reactor was fed KSCN while the other was fed $NH_4(SO_4)_{1/2}$ at equivalent nitrogen loadings in order to mimic the end-products of thiocyanate degradation. Both reactors were also fed molasses (150 mg/L) and KH_2PO_4 (0.28 mM) to provide supplemental nutrients. Feed contained increasing amounts of KOH to modulate reactor pH as necessary (**Figure 1**) and small amounts of 5 N KOH were added directly to reactors if observed pH was ≤ 6.5. Bicarbonate (4 g/L) was added to the feed to buffer the system from day 112 to day 136.

The reactors were run in batch-fed mode until SCN^- degradation was stably observed in the SCN^- reactor, at which time both reactors were switched to continuous feeding at a residence time of 42 hours (day 5). The hydraulic retention time (HRT) of both reactors was lowered from 42 hours to 12 hours (days 5-68) and then maintained at 12 hours while the feed concentration of SCN^- or equivalent $NH_4(SO_4)_{1/2}$ was increased stepwise. The reactor was allowed to stabilize between each step to reach steady state (**Figure S1**).

Sampling: Samples of biomass from each reactor were taken for metagenomic sequencing just before increases in feed concentration (**Figure 1** and **Table S1**). Approximately 0.5 g (wet-weight) of biofilm was scraped from the wall of each reactor with sterile spatula and stored at -60 °C. Paired samples of planktonic biomass were

collected by filtering 300 mL of the liquid phase from each reactor onto a sterile 0.22 µm filter. Biomass was gently washed off the filter with sterile water, pelleted, and stored at -60 °C until further analysis. Filtered media was returned to the reactor to maintain chemical continuity.

Chemical analysis: Bulk liquid was sampled daily for chemical analysis, filtered through a 0.22 µm filter, pH analyzed, and frozen at -20 °C until further analysis. SCN^- was measured using High Performance Liquid Chromatography as described previously.[21] Ion chromatography was performed to quantify nitrate and sulfate (Supporting Information).

DNA extraction and sequencing: DNA was extracted using a NucleoSpin® soil genomic DNA extraction kit (Machery-Nagel, Germany) with the inclusion of a repeated extraction step, according to the manufacturer's instructions. Paired-end Illumina TruSeq libraries with either tight insert fragment sizes of 800 bp or regular insert sizes of 500 bp, depending on the sample, were prepared at the Joint Genome Institute (Walnut Creek, CA) (**Table S1**). Libraries were sequenced on an Illumina HiSeq-2500 in rapid run mode to yield 250 bp paired-end reads.

Metagenomic assembly, binning, and annotation: Reads from each sample were trimmed based on quality scores using sickle (https://github.com/najoshi/sickle) and then assembled independently with idba_ud[23]. Binning of the assembled scaffolds was performed using ggKbase (ggkbase.berkeley.edu) based on scaffold taxonomy, percent GC, and sequencing coverage. Within each assembly, bins were refined and added using differential abundance data visualized in emergent self-organizing maps (ESOMs) as in Sharon *et al.*[24] (see Supplemental Information). Each ESOM was trained and visualized using databionic ESOM tools (**Figure S2**) (http://databionic-esom.sourceforge.net/index.html).[25] In two samples (planktonic inoculum and SCN^- reactor T2 biofilm), subassemblies using $1/60^{th}$ or $1/50^{th}$ of the reads, respectively, were performed to improve assembly of the most abundant organism as previously described by Hug *et al.*[26]

Many bins were redundant given the recurrence of organisms across the time series experiment. Nucmer[27] was used to align sequences and identify sets of bacterial genomes sharing ≥ 98% nucleotide identity across > 50% of the sequence. The best bin was chosen based on genome completeness and length for inclusion in a de-replicated dataset. Genomes without replicates were also included, except for two known contaminant genomes ('Candidatus Altiarchaeum hamiconexum' and an Epsilonproteobacterium) from another sequencing run on the same lane. Bins were excluded from the final de-replicated dataset if they contained < 36 of 51 single copy genes (SCG) or > 8 multi-copy SCG prior to curation (see **Table S2A**). One recurring eukaryotic genome bin, one chloroplast, several mitochondria, phages, eukaryotic viruses, and plasmid bins were included in the de-replicated dataset. De-replicated bacterial genomes were curated using ra2.py, an automated curation method that uses coverage and paired-end read information to find and reassemble or mask regions with mis-assemblies (https://github.com/christophertbrown/fix_assembly_errors/releases/tag/2.00).[28] Curation used the reads of the sample from which the genome originated.

Annotation of genome bins used reciprocal ublast[29] searches against KEGG[30] and UniRef100,[31] as well as single-direction searches against UniProt.[32] Functional genes and marker genes were identified by annotations and using hmmsearch (HMMER 3.1b2; http://hmmer.org/) with Hidden Markov Models (HMMs) from TIGRFAM (v15.0), PFAM,[33] and with custom HMMs[34] (accessible at https://github.com/banfieldlab).

Community composition: Bowtie2 was used with default settings to map reads from each sample to the de-replicated dataset (**Figure S3**). The resulting files were filtered using mapped.py (https://github.com/christophertbrown/mapped) to remove reads that mapped with > 3 mismatches. Coverage for each genome in each sample was calculated and values ≤ 1x were converted to zero. Genome coverage values were then normalized by dividing by the number of reads for each sample and then multiplying by the number of reads in the largest sample. Normalized coverage was used as a proxy for the relative abundances of organisms across samples (**Figure S4**). A concatenated ribosomal protein tree containing references and sequences from SCN^- bioreactors was constructed as previously described[35] (**Figure S5**). Datasets for each of 16 ribosomal proteins were aligned independently with MUSCLE, alignments were trimmed and columns with 99% gaps were removed in Geneious, and trimmed alignments were concatenated. RAxML was used to generate a maximum likelihood phylogeny under the LG + gamma model.

Variant analysis and Replication rate calculations: see Supporting Information.

Protein extraction and proteomic data analysis: Proteins were extracted as previously described[36] and ~1 mg of protein was subjected to trichloroacetic acid precipitation and subsequent digestion with trypsin. Proteolytic peptides were analyzed via an online nano 2D LC–MS/MS system interfaced with hybrid LTQ-Orbitrap-Velos MS (ThermoFisher Scientific). Subsequent processing of the collected spectra was done using Myrimatch[37], with the de-replicated set of genomes as the database (Supporting Information). Peptide identifications were quality-filtered to < 1% false discovery rate. Analysis of proteins involved in key metabolic pathways considered spectral counts for unique peptides and total spectral counts for each protein from two technical replicates.

Data availability: Raw read data is accessible at NCBI under accession number SRP056932 (http://www.ncbi.nlm.nih.gov/sra/SRP056932) and genome accession numbers may be found in **Table S2A**. Genome bins and sequences for scaffolds, genes, and proteins can be viewed and downloaded at http://ggkbase.berkeley.edu/scnpilot-dereplicated/organisms. Proteomics data is available at https://massive.ucsd.edu/ProteoSAFe/datasets.jsp (MassIVE ID MSV000080104).

RESULTS AND DISCUSSION

Reactor chemistry and efficiency: In the newly-inoculated SCN-fed and $NH_4(SO_4)_{1/2}$ reactors, the loading rate was increased across 238 days. Samples were taken for metagenomic analysis after HRT reached 12 h. In the SCN^- reactor, the SCN^- removal rate consistently increased to match the increasing loading rate to a maximum of 1.07 $mmol.h^{-1}$ (**Figures 1A** and **S1A**). On further increase to 1.43 $mmol.h^{-1}$, the SCN^- removal

rate decreased and efficiency dropped to near 50%. On average, the stoichiometry between the SCN^- removal rate and sulfate output was 1.05:1, near the 1:1 ratio expected based on known SCN^- degradation mechanisms coupled to complete oxidation of the sulfide released.

As loading increased, the thickness of the biofilm that formed on all surfaces within the reactor increased. During one period early in the experiment, nitrate (NO_3^-) output reached up to 30% of nitrogen input as SCN^- (days 86-107) and fluctuated thereafter, reaching a maximum of 64% of nitrogen input. After day 200, nitrate output remained consistently low and sulfate accumulated. Base was added periodically to counter acidification as loadings increased. The SCN^- removal rate decreased during one period of high pH that resulted from over-correction of the feed pH (**Figure 1A**).

In the $NH_4(SO_4)_{1/2}$ reactor, the rate of sulfate leaving the reactor rose steadily throughout the experiment, matching the sulfate loading rate and indicating that little sulfate was retained in biomass or converted to other forms (**Figure 1B** and **S1B**). The nitrate output rate increased with decreasing HRT and then increased more slowly as biofilm established and thickened. Overall, higher nitrate effluent concentrations were measured in the $NH_4(SO_4)_{1/2}$ reactor than in the SCN^- reactor (**Figure S1B**).

Genome recovery over the sample series: Biofilm from the two reactors was sampled at four time points (T1-T4) during the experiment, and concurrent samples of planktonic biomass were collected at T2 and T3 in the SCN^- reactor and T2-T4 in the $NH_4(SO_4)_{1/2}$ reactor. The inoculum for these reactors (T0), biofilm and planktonic biomass taken from the SCN^- stock reactor, was also sampled (**Figure 1** and **Table S1**). Independent metagenomic assemblies were performed for each sample and 789 bacterial genome bins were reconstructed (**Figure S2**). Two genomes represented highly abundant organisms, and subassemblies substantially improved these genomes (see Methods). Dereplication across the time-series yielded a non-redundant set of 144 draft-quality genomes (**Tables 1, S2A**). Eukaryotic, mitochondrial, chloroplast, phage and plasmid genomes were also recovered and de-replicated (**Tables 1, S2B**). No Archaea were detected in this system, consistent with previous studies[20-22]. Mapping reads from each assembly demonstrated that this non-redundant genome set accounted for between 72.5 and 93.2% of the data (**Figure S3**). This level of genome recovery approaches that reported for much simpler communities such as those from the infant gut[38]. The de-replicated metagenomic dataset was used as a database for proteomic searches and accounted for 34, 32, and 15% of high-quality peptides from the SCN^- reactor biofilm, $NH_4(SO_4)_{1/2}$ reactor biofilm, and $NH_4(SO_4)_{1/2}$ reactor planktonic samples, respectively, at T4. This level of identification is comparable to that seen with the same type of analysis on infant gut metaproteomes paired to metagenomic databases[39].

Community structure and metabolic potential: Hierarchical clustering of samples based on their community compositions grouped the samples first by the reactor, then by type of biomass and time point from which the samples were taken (**Figure S4**). Clustering organisms by abundance delineated several distinct groups: a small subset of organisms was present in both reactors, while other subsets were found at high-abundance in SCN^- community or the $NH_4(SO_4)_{1/2}$ community. Still other organisms were abundant primarily in the inoculum (**Figure S4**). The taxonomic identity of

genomes was determined via phylogenetic reconstruction using ribosomal proteins (**Figure S5**). In order to identify key organisms in the bioreactor communities, we characterized the metabolic potential encoded and expressed by each genome with respect to the key processes of SCN^- degradation, sulfur, ammonium, and nitrite oxidation, denitrification, and carbon fixation (**Figure S4**, **Table S2A**).

SCN^- removal and sulfur cycling: Four genomes, Thiobacillus_1, Thiobacillus_3, Thiobacillus_4 and Afipia_1, contain one of two known types of SCN^- hydrolases[11,40]. The corresponding organisms were abundant only in the SCN^- reactor (**Figure 2**), and proteomics data support activity of these organisms in SCN^- degradation, sulfur oxidation and carbon fixation (**Figure 3**). Peptides detected by proteomics matched to predicted proteins in the recently described SCN^- operon from *Thiobacillus* spp.[21] Specifically, the genes in the operon were detected by proteomics with spectral hits in at least one of the three *Thiobacillus* genomes that contained this operon. Interestingly, an SQR-like protein in this operon had the highest count of unique spectral hits for all three genomes (**Table S3**). The cbiM-like protein hypothesized to be involved in cobalt metabolism was the only protein from the operon not detected in proteomics.

Consistent with the genome of *Thiobacillus denitrificans,*[41] all six recovered *Thiobacillus* genomes encode the potential for autotrophic growth on sulfur compounds via numerous sulfur-related genes from multiple pathways (**Table S2A**). In a transcriptomics-based study of *Thiobacillus denitrificans*, some of these genes were constitutively expressed (*sox*, *rDsr*, *apr*, *atps*) whereas others are upregulated under denitrifying conditions (e.g., sulfide quinone reductase).[42] We identified all sulfur oxidation genes in proteomics for several of the Thiobacilli described here (**Figure 3**).

In addition to the four genomes encoding thiocyanate-degradation, twenty-two other genomes possess the Sox pathway (including at least 4 of *soxX*, *Y*, *Z*, *A*, and *B*, with or without *soxCD*; **Table S2A**). Of these, the genomes with the highest normalized coverages in the SCN^- reactor were Burkholderiales_6, Thiobacillus_2 and Rhizobiales_3 (**Figure 2**). Sulfur oxidation may proceed from sulfide to elemental sulfur or sulfate, likely determined by the availability of electron acceptors, as discussed below. Sulfur globules may be produced by SCN-degrading *Thiobacillus* spp., which use the reverse dissimilatory sulfite reductase (rDsr) pathway instead of soxCD[43]. In turn, other sulfur oxidizers may use this elemental sulfur and any excess sulfide produced by SCN^- degradation. Since chemical data showed that SCN^- was completely converted to sulfate, and proteomic data showed expression of Sox proteins from genomes lacking known thiocyanate hydrolases (**Figure 3**), we suspect that sulfur species were passed from SCN-degraders to the rest of community as "metabolic handoffs". Additionally, some of these organisms may use as-yet-unidentified pathways for SCN^- degradation.

Community dynamics and SCN^- removal across increased loadings: As SCN^- loadings and SCN^- degradation rate increased (**Figure 1**), the relative abundance of *Thiobacillus* spp. whose genomes encode SCN-degradation also increased (**Figure 2**), with Thiobacillus_1 alone accounting for 38% of all reads at T2. During operation at the two final loading rates (T3 and T4), the Thiobacillus_1 population decreased in relative abundance, concordant with a decrease in SCN^- degradation rate and reactor efficiency.

Given this observation, we looked for other changes associated with loss of reactor efficiency.

First, a read mapping-based sequence variance analysis of the Thiobacillus_1 population in each sample showed that it was largely clonal throughout the time series but two distinct strains were present at the last time point, where the relative strain proportions were ~60 and 40% (**Figures S6A** and **S6B)**. The genome for the second strain was not recovered, but a scaffold corresponding to the SCN^- operon was identified among the un-binned metagenomic data from this time point. We noted a few differences in the protein sequences of genes contained in this operon, which could in principle affect the efficiency of SCN^- degradation relative to the dominant strain (**Figure S7**).

A second change in the community was the increase in relative abundance of Burkholderiales_6, which became dominant in T3 and T4 (**Figure S8**). No known genes for SCN^- degradation were found in the Burkholderiales_6 genome, but previous studies have isolated and characterized a strain of *Burkholderia phytofirmans* capable of thiocyanate degradation with acetate as a carbon source.[44] The genome of Burkholderiales_6 contains genes encoding the *sox* pathway, and the corresponding proteins were detected in proteomics (**Figure 3**). Hence we infer that the Burkholderiales_6 organism likely used reduced sulfur species for mixotrophic growth, and may have increased in relative abundance concordant with the accumulation of organic matter in the reactor (in the form of biomass), perhaps outcompeting Thiobacillus_1 for SCN^- as a source of nitrogen and energy. Overall, the results suggest a transition from autotrophic to mixotrophic / heterotrophic thiocyanate degradation at high thiocyanate loadings and after long periods of reactor operation.

A third change in the reactor community that could have affected SCN^- degradation was substantial algal growth at the last time point. This was visually observed in the planktonic portion of the SCN^- reactor and could have affected microbial population dynamics and reactor efficiency. Lastly, the increase in residual SCN^- concentrations in the reactor may have led to toxicity effects including lower bacterial replication rates (see below). This in turn could have reduced the SCN^- degradation rate, creating a negative feedback effect on reactor performance.

Overall, we speculate that the decline in reactor efficiency at high loading rates occurred when the capacity for SCN^- degradation was exceeded. The abundance of *Thiobacillus* cells may have been insufficient to meet the demand for SCN^- degradation owing to a maximum specific SCN^- degradation rate. Alternatively, degradation may have been inhibited or the per-cell rate of degradation may have decreased. Since metagenomic data provide relative abundance information, the apparent decrease in Thiobacillus_1 relative abundance may have been due to increases in abundance of other organisms, such as Burkholderiales_6. Further studies are needed that apply measurements of absolute, species-specific biomass and metabolic rates.

Nitrogen removal and dynamics over time: Since SCN^- degradation releases nitrogen in the form of ammonium, we looked for possible mechanisms of nitrogen cycling and removal to N_2. No anamox genes were detected in any genome and, based on identified genes and genomes, the conversion of ammonium to nitrate occurred aerobically. A single genome in the dataset, Nitrosospira_1, encoded the potential for ammonium oxidation (**Figure S4**). The Nitrosospira_1 organism became enriched at early time points

in the $NH_4(SO_4)_{1/2}$ reactor and later in the SCN^- reactor (**Figure 2**) and was active at the final time point, based on proteomic data (**Figure 3**). Two predicted nitrite oxidizers, Nitrobacter_1 and Nitrobacter_2, were present at low abundances in the $NH_4(SO_4)_{1/2}$ reactor (**Figure 2**) and were so low in abundance in the SCN^- reactor that their genomes did not assemble. However, proteins for nitrite oxidation corresponding to one of these genomes were detected in samples from both reactors (**Figure 3**). Low abundance but high activity has been observed previously for other nitrite oxidizing bacteria, and some have hypothesized that high nitrite oxidation activity may be a requirement for growth, given the low energy yield of this metabolism.[45] Despite the low relative abundance of both predicted ammonium and nitrite oxidizers, nitrate was detected in the effluent of both reactors during the initial ramping phases (**Figure 1**).

Searching for mechanisms of nitrate removal, we identified 92 genomes that contained at least one gene involved in denitrification (including *nar*, *nap*, *nirS*, *nirK*, *norB*/*norZ*, and *nosZ*; **Table S2A**). Fourteen of these genomes encoded the capacity for complete nitrate reduction to N_2, whereas 49 had only one gene in the pathway. Genomes of complete denitrifiers corresponded to three of the predicted autotrophs implicated in SCN^- removal: Thiobacillus_1, Thiobacillus_3, and Afipia_1 (**Figure 2**). For the Thiobacilli, several denitrification-related complexes were detected with proteomics (**Figure 3**). SCN^- hydrolysis and concomitant sulfide oxidation coupled to denitrification may be possible in these organisms, as was described for *Thioalkalivibrio*.[46] Based on proteomic evidence, the Burkholderiales_6 organism, which became abundant in T3 and T4 in the SCN^- reactor, also likely contributed to denitrification (**Figure 2** and **3**). All denitrification genes except *norB* were identified in proteomics from the SCN^- reactor biofilm (**Figure 3**). The limited detection of NorB may be an extraction bias artifact due to numerous transmembrane domains in these proteins.[47,48]

In the $NH_4(SO_4)_{1/2}$ reactor, three of most abundant bacteria, Rhodanobacter_1, Xanthomonadales_1, and Novosphingobium_1 may have roles in denitrification (**Figure 2** and **Table S2A**). The potential for dissimilatory nitrate reduction to ammonia (via *nrfA)* was detected in genomes from several members of the Bacteroidetes and one *Aeromonas* sp. but most of these were abundant only in the inoculum (**Table S2A**) and NrfA was not detected in the proteomic data.

Changes in bacterial replication rates across the time series: We used a recently established approach to investigate bacterial replication rates from metagenomics[49] with a new implementation that reports rates as index of replication (iRep) values.[50] In the SCN^- reactor biofilm, iRep values for most genomes increased between T0 and T1, suggesting replication proceeded more quickly in newly-forming biofilm than in inoculum biofilm taken from the long-running SCN^- stock reactor (**Figure S7**). Over the remainder of the experiment (T2-T4), iRep values decreased for most genomes, especially toward the end of the experiment. This may have been due to toxicity of residual SCN^- in the reactor media or to spatial limitations for growth within the thickening biofilm.

In contrast, iRep values in the $NH_4(SO_4)_{1/2}$ reactor biofilm were initially low, but increased from T1 to T3. This is suggestive of a period of adaptation, as organisms adjusted to the new conditions relative to the SCN^- stock reactor (**Figure S9**).

Biofilm and planktonic communities: The planktonic and biofilm portions of the reactor were sampled separately in order to understand whether these represented distinct communities. At T1, the planktonic fraction of each reactor was very dilute, yielding inadequate amounts of DNA for sequencing, and at T4, the planktonic portion of the SCN^- reactor was overgrown with algae. At T2, metagenomes for planktonic samples from both reactors were highly enriched in a rotifer genome, which accounted for 45 and 25 % of the sequence data in the $NH_4(SO_4)_{1/2}$ and SCN^- reactors, respectively. With microscopy, rotifers were observed grazing on biofilm (**Figure S10**). Other eukaryotes were observed in both reactors, and many of these organisms were at higher relative abundance in the planktonic samples compared to biofilm (**Table S2**). Recurring mitochondrial sequences recovered in the metagenomes corresponded to relatives of *Vermamoeba vermiformis*, *Acanthamoeba* spp., *Naegleria fowleri*, and *Chlorella* sp., identified based on the phylogenetic profile of their proteins and searches against NCBI-nr (**Table S2B**).

Eleven bacterial genomes in the dataset derived from predicted symbionts, as indicated by their phylogenetic affiliations and/or reduced genome sizes (**Figure S4** and **Table S2A**). These included two complete genomes for organisms belonging to the phylum Saccharibacteria[51,52] (formerly TM7). One organism, TM7_2, was the only putative symbiont found at high abundances in planktonic fractions of both reactors (**Figure 2**).

Overall, we estimate that biofilm constituted the majority of the biomass in the reactors, and sloughing may have contributed to the planktonic community. While SCN^- degradation itself does not rely on biofilm,[53,54] the formation of biofilm effectively uncoupled the HRT from bacterial growth rates, preventing wash-out as the HRT was decreased. This may have allowed *Thiobacillus* spp., and nitrifiers to reach higher population sizes than would otherwise have been possible, thereby converting higher loadings of SCN^- to nitrate. The biofilm likely also provided anoxic conditions promoting denitrification, as suggested by proteomic data (see above).

Long-term community stability and phage susceptibility: We compared the 114 bacterial genomes in this study to 86 genomes reconstructed in a prior study of the SCN^- stock reactor and a daughter reactor fed cyanide and SCN^- (CN-SCN reactor) conducted two years earlier.[21] Thirty-one genomes were matched, overlapping by at least a total of 1 Mbp at 98% nucleotide identity (**Table S2A**). These included close relatives of the three SCN-degrading *Thiobacillus* spp. and Burkholderiales_6 enriched in the SCN-treated reactor studied here. Given the importance of these three populations, we looked for evidence of recent phage infections, based on changes to CRISPR loci over time. Thiobacillus_1 has no CRISPR locus, perhaps making it more susceptible to acquisition of mobile elements and phage attack. The CRISPR locus in Thiobacillus_3 was identical in all versions of this genome recovered from the current study, but was not recovered in the previous study. The recovered Thiobacillus_4 genomes belonged to two distinct CRISPR sub-types that differed from one another in 12 spacers at the 3' end of the array: sequences from biofilm and planktonic inoculum samples comprised one version, and sequences from later in the time series (and those recovered previously in the SCN^- stock reactor and the CN-SCN reactor) comprised the second version. Importantly, no spacers from Thiobacillus_3 and Thiobacillus_4 targeted any sequence in the metagenomes (or

previous metagenomes from the SCN^- stock or CN-SCN reactors), suggesting little recent phage interaction.

System overview: Relatives of known SCN-degrading chemolithoautotrophs (several *Thiobacillus* spp. and one *Afipia* sp.) are predicted to oxidize the SCN-sulfur as their sole energy source under both aerobic and anaerobic conditions in the SCN^- reactor (**Figure 4A**). Sulfide oxidation may stop at elemental sulfur when parts of the reactor become anaerobic[55] (**Figure 4B**), and proteomic data suggest that several *Thiobacillus* spp., as well as Burkholderiales_6, coupled sulfur oxidation to denitrification (**Figure 3**). In fact, based on their abundance, and proteomic evidence, these organisms may be the key denitrifiers in the system. Other sulfur oxidizing autotrophs and mixotrophs may use reduced sulfur compounds produced during SCN^- degradation, including elemental sulfur. The combination of sulfide oxidation by SCN-degraders and non-degraders may explain the complete conversion of sulfur from SCN^- to sulfate (**Figure 4B)**. The breakdown of SCN^- produces ammonium that can be converted to nitrate by autotrophic ammonium and nitrite oxidizers. Overall, some heterotrophs in the system likely contributed to sulfur oxidation and denitrification, and likely also to biofilm formation and biofilm integrity (perhaps via filamentous morphology, see **Figure S10**). Heterotrophs may also break down SCN^- as a source of nitrogen (via an unknown pathway).[44] However, this SCN^- degradation may be inhibited if there is abundant nitrogen available as ammonium, as observed in some alkaliphiles.[15] Lastly, eukaryotes such as rotifers and amoeba are predators and thus contribute to carbon turnover in the system.

Engineering of SCN^- degradation by a microbial community: The consortium described here can completely hydrolyze SCN^- and oxidize sulfide under a range of SCN^- loadings but reduced performance occurred at higher loadings. Smaller increases in concentration to reach higher loadings may lead to sustained reactor performance by allowing microbial cell numbers and associated volumetric degradation rates to keep pace with input SCN^-. For treating such high SCN^- concentrations at low retention times (>12.9 mM or 750 ppm in 12 hours), an attached growth design may have better SCN^- and nitrogen removal.

Studies on such biofilm-based systems for SCN^- treatment have demonstrated the effectiveness of rotating biological contact (RBC)[56,57] and fixed bed and fluidized-carrier type reactors.[58,59] Potential weaknesses of these systems include biofilm overgrowth leading to poor mixing and aeration. The ASTER™ process, modeled here with laboratory-scale CSTRs, was designed to be easy to establish at remote locations and to accommodate suspended solid tailings when necessary.[53,54] The results of our work on a laboratory-scale CSTR suggest that biofilm can play an important role when this reactor design is operated at high loadings.

Our work highlights the applicability of bioinformatics tools to gain a mechanistic understanding of contaminant degradation by a microbial community, to assess community stability, and ultimately, to inform engineering design choices. Others have called for broader use of metagenomics to advance biotechnology, including in wastewater treatment,[60,61] and this study represents a step toward the use of such techniques in the field. The level of resolution achieved using metagenomics combined

with metaproteomics allowed us to access not only phylogenetic classifications and diversity of community members, but also which members express key proteins involved in the degradation process. The dataset and analysis provide valuable information that can be used to generate primers or probes for on-site measurements.

ACKNOWLEDGEMENTS

We gratefully acknowledge assistance from Alexander Probst, Andrea Singh, Spencer Diamond, Paula Matheus-Carnavali, A. Wynand Van Zyl, Robert Van Hille, Tanya Hodgson, and Tijana Glavina del Rio. Funding was provided by an NSF Sustainable Chemistry grant (1349278), NSF-GRFP and NSF-GROW with USAID fellowships to RSK, the Department of Science and Technology (DST) and NRF of South Africa through the SARChI Chair in Bioprocess Engineering (UID 64778), and an NRF Research Career Advancement Fellowship to RJH. Oak Ridge National Lab received support from the U.S. Department of Energy, Genome Science Program. The Joint Genome Institute Emerging Technologies Opportunity Program provided sequencing, and was in turn supported by the Office of Science of the U.S. Department of Energy under Contract No. DE-AC02-05CH11231.

SUPPORTING INFORMATION AVAILABLE

This information is available free of charge at http://pubs.acs.org.

AUTHOR CONTRIBUTIONS

RSK, RJH, STLH, and JFB designed the study; RSK and JFB wrote the paper; all co-authors read and contributed to revisions of the paper; RJH operated and sampled the bioreactors and conducted analysis for metadata, with contributions from STLH; SGT provided DNA sequencing; RI and RLH collected and processed proteomic data; RSK analyzed metagenomic and proteomic data with contributions from BCT, CTB, and KA.

FIGURES AND TABLES

Table 1. Counts and completeness estimated by single copy gene (SCG) inventories for de-replicated bins resulting from 15 metagenome assemblies.

Bacterial genomes (144)	**Count**
Genomes ≥ 96% complete (49/51 SCG)	111
Genomes in ≤ 30 scaffolds and 49/51 SCG	37
Genomes with ≥ 90% of sequence in scaffolds > 10 kb	117
Non-bacterial bins (90)	**Count**
Plasmids and mobile elements	45
Phage	25
Eukaryotes	1
Mitochondria	15
Chloroplasts	1
Viruses	3

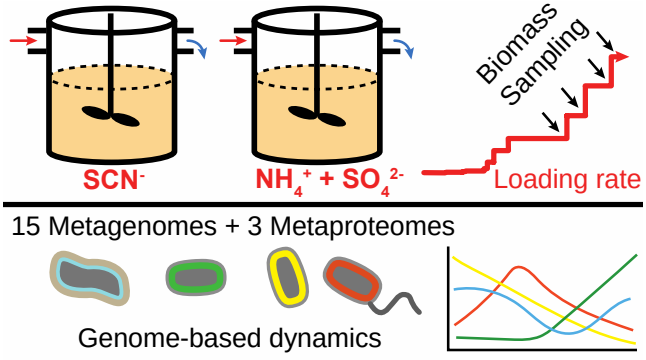

TOC/Abstract art

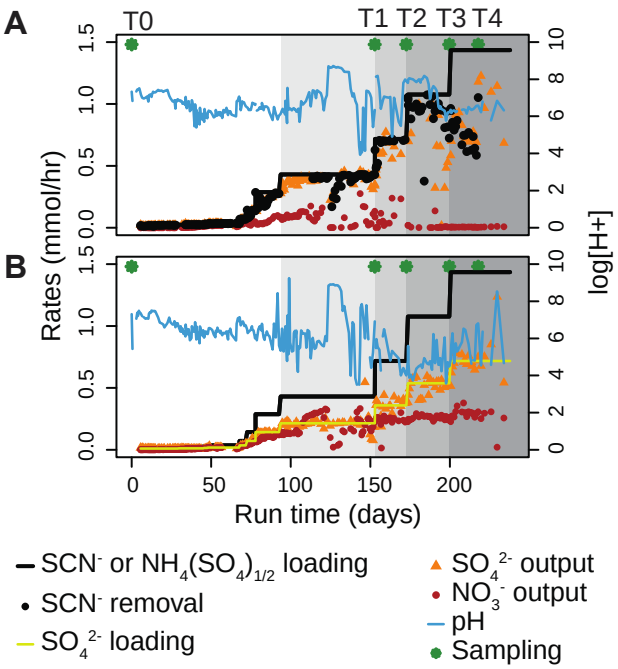

Figure 1. Chemical parameters of operation for the SCN^- reactor (**A**), and $NH_4(SO_4)_{1/2}$ reactor (**B**). Sampling time points are indicated above plots. Gray shading indicates the different loading regimes.

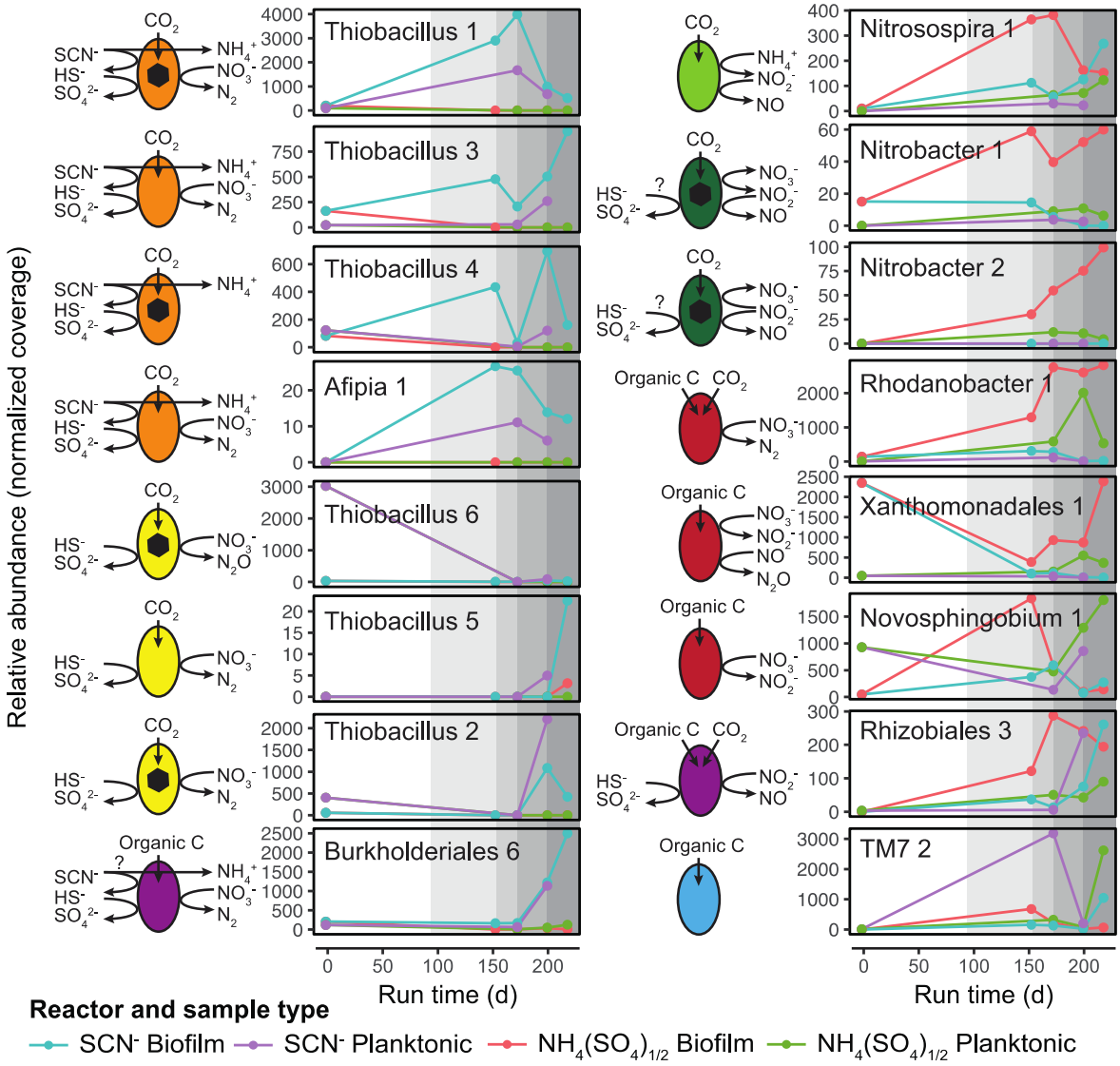

Figure 2. Metabolic potential and relative abundances of key organisms of interest over time in biofilm and planktonic samples from both reactors. Gray shading corresponds to increasing loading rates of SCN^- or $NH_4(SO_4)_{1/2}$ as in Figure 1. SCN^- degraders (orange) and several key sulfur oxidizers (yellow and purple) were found at higher relative abundance in the SCN^- reactor while ammonium and nitrite oxidizers (green) were at higher relative abundances in the $NH_4(SO_4)_{1/2}$ reactor. Several highly abundant heterotrophs (red and blue) and one possible sulfur oxidizing mixotroph (purple) were present in both reactors. Note different y-axis scales. Hexagons indicate carboxysomes where annotations support this prediction.

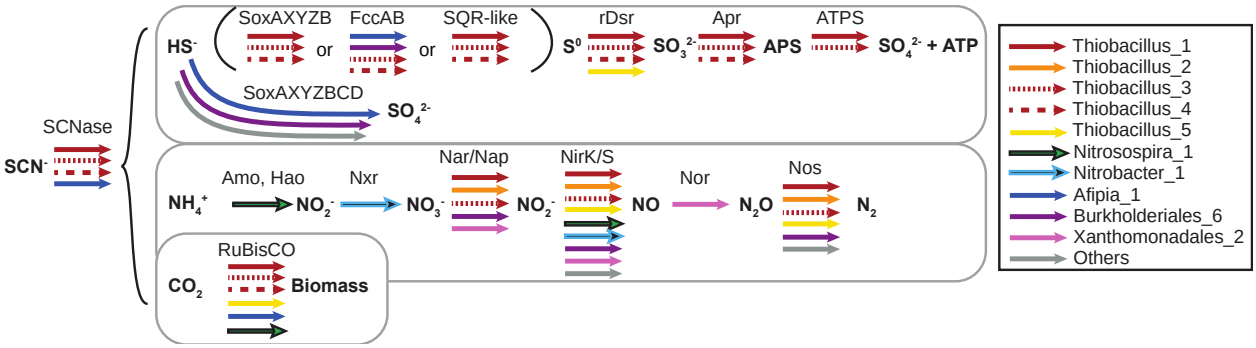

542
543 **Figure 3.** Metaproteomics at end point (T4) in SCN^- reactor shows expression of
544 genes involved in SCN^- degradation and byproduct breakdown in key organisms.
545 Each arrow indicates that the average of unique spectral counts across two technical
546 replicates was ≥ 2 for at least one subunit or component of the enzyme complex
547 involved in the chemical transformation.
548
549

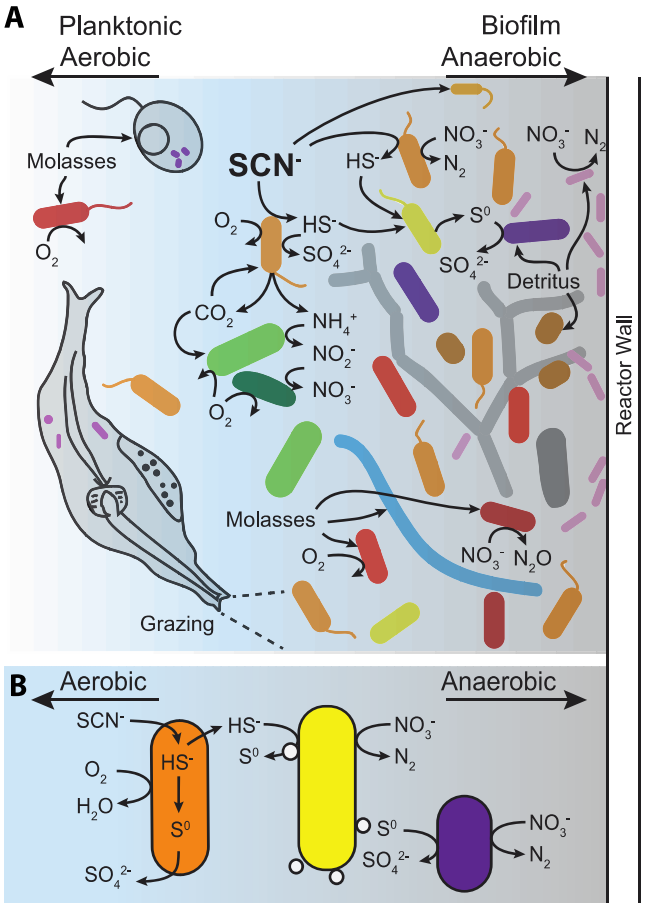

Figure 4. SCN^- removal and sulfur, nitrogen, and carbon cycling in the reactor system depicted based on metagenomic analysis.

LITERATURE CITED

(1) Speth, D. R.; In 't Zandt, M. H.; Guerrero-Cruz, S.; Dutilh, B. E.; Jetten, M. S. M. Genome-based microbial ecology of anammox granules in a full-scale wastewater treatment system. *Nature Communications* **2016**, *7*, 11172.

(2) Sekiguchi, Y.; Ohashi, A.; Parks, D. H.; Yamauchi, T.; Tyson, G. W.; Hugenholtz, P. First genomic insights into members of a candidate bacterial phylum responsible for wastewater bulking. *PeerJ* **2015**, *3*, e740.

(3) Albertsen, M.; Saunders, A. M.; Nielsen, K. L.; Nielsen, P. H. Metagenomes obtained by "deep sequencing" – what do they tell about the enhanced biological phosphorus removal communities? *Water Sci. Technol.* **2013**, *68* (9), 1959.

(4) Hug, L. A.; Beiko, R. G.; Rowe, A. R.; Richardson, R. E.; Edwards, E. A. Comparative metagenomics of three Dehalococcoides-containing enrichment cultures: the role of the non-dechlorinating community. *BMC Genomics* **2012**, *13* (1), 327.

(5) Lykidis, A.; Chen, C.-L.; Tringe, S. G.; McHardy, A. C.; Copeland, A.; Kyrpides, N. C.; Hugenholtz, P.; Macarie, H.; Olmos, A.; Monroy, O.; et al. Multiple syntrophic interactions in a terephthalate-degrading methanogenic consortium. *The ISME Journal* **2010**, *5* (1), 122–130.

(6) Nobu, M. K.; Narihiro, T.; Rinke, C.; Kamagata, Y.; Tringe, S. G.; Woyke, T.; Liu, W.-T. Microbial dark matter ecogenomics reveals complex synergistic networks in a methanogenic bioreactor. *The ISME Journal* **2015**, *9* (8), 1710–1722.

(7) Taubert, M.; Vogt, C.; Wubet, T.; Kleinsteuber, S.; Tarkka, M. T.; Harms, H.; Buscot, F.; Richnow, H.-H.; Bergen, von, M.; Seifert, J. Protein-SIP enables time-resolved analysis of the carbon flux in a sulfate-reducing, benzene-degrading microbial consortium. *The ISME Journal* **2012**, *6* (12), 2291–2301.

(8) Erdogan, M. F. Thiocyanate overload and thyroid disease. *Biofactors* **2003**, *19* (3-4), 107–111.

(9) Speyer, M. R.; Raymond, P. The acute toxicity of thiocyanate and cyanate to rainbow trout as modified by water temperature and pH. *Environmental Toxicology and Chemistry* **1988**, *7* (7), 565–571.

(10) Watson, S. J.; Maly, E. J. Thiocyanate toxicity to *Daphnia magna*: modified by pH and temperature. *Aquatic Toxicology* **1987**, *10* (1), 1–8.

(11) Hussain, A.; Ogawa, T.; Saito, M.; Sekine, T.; Nameki, M.; Matsushita, Y.; Hayashi, T.; Katayama, Y. Cloning and expression of a gene encoding a novel thermostable thiocyanate-degrading enzyme from a mesophilic alphaproteobacteria strain THI201. *Microbiology* **2013**, *159* (Pt 11), 2294–2302.

(12) Katayama, Y.; Kuraishi, H. Characteristics of *Thiobacillus thioparus* and its thiocyanate assimilation. *Can. J. Microbiol.* **1978**, *24* (7), 804–810.

(13) Katayama, Y.; Narahara, Y.; Inoue, Y.; Amano, F.; Kanagawa, T.; Kuraishi, H. A thiocyanate hydrolase of Thiobacillus thioparus. A novel enzyme catalyzing the formation of carbonyl sulfide from thiocyanate. *J. Biol. Chem.* **1992**, *267* (13), 9170–9175.

(14) Katayama, Y.; Matsushita, Y.; Kaneko, M.; Kondo, M.; Mizuno, T.; Nyunoya, H. Cloning of genes coding for the three subunits of thiocyanate hydrolase of

Thiobacillus thioparus THI 115 and their evolutionary relationships to nitrile hydratase. *Journal of Bacteriology* **1998**, *180* (10), 2583–2589.

(15) Sorokin, D. Y.; Tourova, T. P.; Lysenko, A. M.; Kuenen, J. G. Microbial thiocyanate utilization under highly alkaline conditions. *Applied and Environmental Microbiology* **2001**, *67* (2), 528–538.

(16) Stratford, J.; Dias, A. E.; Knowles, C. J. The utilization of thiocyanate as a nitrogen source by a heterotrophic bacterium: the degradative pathway involves formation of ammonia and tetrathionate. *Microbiology (Reading, Engl.)* **1994**, *140*, 2657–2662.

(17) Wood, A. P.; Kelly, D. P.; McDonald, I. R.; Jordan, S. L.; Morgan, T. D.; Khan, S.; Murrell, J. C.; Borodina, E. A novel pink-pigmented facultative methylotroph, *Methylobacterium thiocyanatum* sp. nov., capable of growth on thiocyanate or cyanate as sole nitrogen sources. *Arch Microbiol* **1998**, *169* (2), 148–158.

(18) Boucabeille, C.; Bories, A.; Ollivier, P.; Michel, G. Microbial degradation of metal complexed cyanides and thiocyanate from mining wastewaters. *Environ. Pollut.* **1994**, *84* (1), 59–67.

(19) van Buuren, C.; Makhotla, N.; Olivier, J. W. The ASTER process: technology development through to piloting, demostration, and comercialization. *Proceedings of the ALTA 2011 Nickel-Cobalt-Copper, Uranium and Gold Conference* **2011**.

(20) Huddy, R. J.; van zyl, A. W.; van Hille, R. P.; Harrison, S. T. L. Characterisation of the complex microbial community associated with the ASTER^{TM} thiocyanate biodegradation system. *Minerals Engineering* **2015**, *76*, 65–71.

(21) Kantor, R. S.; van zyl, A. W.; van Hille, R. P.; Thomas, B. C.; Harrison, S. T. L.; Banfield, J. F. Bioreactor microbial ecosystems for thiocyanate and cyanide degradation unravelled with genome-resolved metagenomics. *Environ Microbiol* **2015**, *17* (12), 4929–4941.

(22) van Zyl, A. W.; Harrison, S. T. L.; van Hille, R. P. Biodegradation of thiocyanate by a mixed microbial population. *Proceedings of the International Mine Water Association Conference, 2011* **2011**, 119–124.

(23) Peng, Y.; Leung, H. C. M.; Yiu, S. M.; Chin, F. Y. L. IDBA-UD: a de novo assembler for single-cell and metagenomic sequencing data with highly uneven depth. *Bioinformatics* **2012**, *28* (11), 1420–1428.

(24) Sharon, I.; Morowitz, M. J.; Thomas, B. C.; Costello, E. K.; Relman, D. A.; Banfield, J. F. Time series community genomics analysis reveals rapid shifts in bacterial species, strains, and phage during infant gut colonization. *Genome Research* **2013**, *23* (1), 111–120.

(25) Ultsch, A.; Mörchen, F. ESOM-Maps: tools for clustering, visualization, and classification with Emergent SOM. *Data Bionics Research Group, University of Marburg, Germany* **2005**.

(26) Hug, L. A.; Thomas, B. C.; Sharon, I.; Brown, C. T.; Sharma, R.; Hettich, R. L.; Wilkins, M. J.; Williams, K. H.; Singh, A.; Banfield, J. F. Critical biogeochemical functions in the subsurface are associated with bacteria from new phyla and little studied lineages. *Environ Microbiol* **2016**, *18* (1), 159–173.

(27) Kurtz, S.; Phillippy, A.; Delcher, A. L.; Smoot, M.; Shumway, M.; Antonescu, C.; Salzberg, S. L. Versatile and open software for comparing large genomes.

Genome Biol **2004**, *5* (2), R12.
(28) Brown, C. T.; Hug, L. A.; Thomas, B. C.; Sharon, I.; Castelle, C. J.; Singh, A.; Wilkins, M. J.; Wrighton, K. C.; Williams, K. H.; Banfield, J. F. Unusual biology across a group comprising more than 15% of domain Bacteria. *Nature* **2015**, *523* (7559), 208–211.
(29) Edgar, R. C. Search and clustering orders of magnitude faster than BLAST. *Bioinformatics* **2010**, *26* (19), 2460–2461.
(30) Kanehisa, M.; Sato, Y.; Kawashima, M.; Furumichi, M.; Tanabe, M. KEGG as a reference resource for gene and protein annotation. *Nucleic Acids Research* **2016**, *44* (D1), D457–D462.
(31) Suzek, B. E.; Wang, Y.; Huang, H.; McGarvey, P. B.; Wu, C. H.; The UniProt Consortium. UniRef clusters: a comprehensive and scalable alternative for improving sequence similarity searches. *Bioinformatics* **2015**, *31* (6), 926–932.
(32) The UniProt Consortium. UniProt: a hub for protein information. *Nucleic Acids Research* **2015**, *43* (D1), D204–D212.
(33) Finn, R. D.; Coggill, P.; Eberhardt, R. Y.; Eddy, S. R.; Mistry, J.; Mitchell, A. L.; Potter, S. C.; Punta, M.; Qureshi, M.; Sangrador-Vegas, A.; et al. The Pfam protein families database: towards a more sustainable future. *Nucleic Acids Research* **2016**, *44* (D1), D279–D285.
(34) Anantharaman, K.; Brown, C. T.; Hug, L. A.; Sharon, I.; Castelle, C. J.; Probst, A. J.; Thomas, B. C.; Singh, A.; Wilkins, M. J.; Karaoz, U.; et al. Thousands of microbial genomes shed light on interconnected biogeochemical processes in an aquifer system. *Nature Communications* **2016**, *7*, 13219.
(35) Hug, L. A.; Castelle, C. J.; Wrighton, K. C.; Thomas, B. C.; Sharon, I.; Frischkorn, K. R.; Williams, K. H.; Tringe, S. G.; Banfield, J. F. Community genomic analyses constrain the distribution of metabolic traits across the Chloroflexi phylum and indicate roles in sediment carbon cycling. *Microbiome* **2013**, *1* (1), 22.
(36) Chourey, K.; Jansson, J.; VerBerkmoes, N.; Shah, M.; Chavarria, K. L.; Tom, L. M.; Brodie, E. L.; Hettich, R. L. Direct Cellular Lysis/Protein Extraction Protocol for Soil Metaproteomics. *J. Proteome Res.* **2010**, *9* (12), 6615–6622.
(37) Tabb, D. L.; Fernando, C. G.; Chambers, M. C. MyriMatch: highly accurate tandem mass spectral peptide identification by multivariate hypergeometric analysis. *J. Proteome Res.* **2007**, *6* (2), 654–661.
(38) Raveh-Sadka, T.; Thomas, B. C.; Singh, A.; Firek, B.; Brooks, B.; Castelle, C. J.; Sharon, I.; Baker, R.; Good, M.; Morowitz, M. J.; et al. Gut bacteria are rarely shared by co-hospitalized premature infants, regardless of necrotizing enterocolitis development. *eLife* **2015**, *4*.
(39) Xiong, W.; Giannone, R. J.; Morowitz, M. J.; Banfield, J. F.; Hettich, R. L. Development of an enhanced metaproteomic approach for deepening the microbiome characterization of the human infant gut. *J. Proteome Res.* **2015**, *14* (1), 133–141.
(40) Arakawa, T.; Kawano, Y.; Kataoka, S.; Katayama, Y.; Kamiya, N.; Yohda, M.; Odaka, M. Structure of Thiocyanate Hydrolase: A New Nitrile Hydratase Family Protein with a Novel Five-coordinate Cobalt(III) Center. *Journal of Molecular Biology* **2007**, *366* (5), 1497–1509.

(41) Beller, H. R.; Chain, P. S. G.; Letain, T. E.; Chakicherla, A.; Larimer, F. W.; Richardson, P. M.; Coleman, M. A.; Wood, A. P.; Kelly, D. P. The genome sequence of the obligately chemolithoautotrophic, facultatively anaerobic bacterium *Thiobacillus denitrificans*. *Journal of Bacteriology* **2006**, *188* (4), 1473–1488.

(42) Beller, H. R.; Letain, T. E.; Chakicherla, A.; Kane, S. R.; Legler, T. C.; Coleman, M. A. Whole-genome transcriptional analysis of chemolithoautotrophic thiosulfate oxidation by *Thiobacillus denitrificans* under aerobic versus denitrifying conditions. *Journal of Bacteriology* **2006**, *188* (19), 7005–7015.

(43) Loy, A.; Duller, S.; Baranyi, C.; Mussmann, M.; Ott, J.; Sharon, I.; Béjà, O.; Le Paslier, D.; Dahl, C.; Wagner, M. Reverse dissimilatory sulfite reductase as phylogenetic marker for a subgroup of sulfur-oxidizing prokaryotes. *Environ Microbiol* **2009**, *11* (2), 289–299.

(44) Vu, H. P.; Mu, A.; Moreau, J. W. Biodegradation of thiocyanate by a novel strain of *Burkholderia phytofirmans* from soil contaminated by gold mine tailings. *Lett. Appl. Microbiol.* **2013**, *57* (4), 368–372.

(45) Baker, B. J.; Sheik, C. S.; Taylor, C. A.; Jain, S.; Bhasi, A.; Cavalcoli, J. D.; Dick, G. J. Community transcriptomic assembly reveals microbes that contribute to deep-sea carbon and nitrogen cycling. *The ISME Journal* **2013**, *7* (10), 1962–1973.

(46) Sorokin, D. Y.; Tourova, T. P.; Antipov, A. N.; Muyzer, G.; Kuenen, J. G. Anaerobic growth of the haloalkaliphilic denitrifying sulfur-oxidizing bacterium *Thialkalivibrio thiocyanodenitrificans* sp. nov. with thiocyanate. *Microbiology (Reading, Engl.)* **2004**, *150* (Pt 7), 2435–2442.

(47) Hino, T.; Matsumoto, Y.; Nagano, S.; Sugimoto, H.; Fukumori, Y.; Murata, T.; Iwata, S.; Shiro, Y. Structural basis of biological N_2O generation by bacterial nitric oxide reductase. *Science* **2010**, *330* (6011), 1666–1670.

(48) Matsumoto, Y.; Tosha, T.; Pisliakov, A. V.; Hino, T.; Sugimoto, H.; Nagano, S.; Sugita, Y.; Shiro, Y. Crystal structure of quinol-dependent nitric oxide reductase from *Geobacillus stearothermophilus*. *Nat Struct Mol Biol* **2012**, *19* (2), 238–245.

(49) Korem, T.; Zeevi, D.; Suez, J.; Weinberger, A.; Avnit-Sagi, T.; Pompan-Lotan, M.; Matot, E.; Jona, G.; Harmelin, A.; Cohen, N.; et al. Growth dynamics of gut microbiota in health and disease inferred from single metagenomic samples. *Science* **2015**, *349* (6252), 1101–1106.

(50) Brown, C. T.; Olm, M. R.; Thomas, B. C.; Banfield, J. F. Measurement of bacterial replication rates in microbial communities. *Nature biotechnology* **2016**.

(51) Bor, B.; Poweleit, N.; Bois, J. S.; Cen, L.; Bedree, J. K.; Zhou, Z. H.; Gunsalus, R. P.; Lux, R.; McLean, J. S.; He, X.; et al. Phenotypic and physiological characterization of the epibiotic interaction between TM7x and its basibiont *Actinomyces*. *Microb Ecol* **2015**, *71* (1), 243–255.

(52) He, X.; McLean, J. S.; Edlund, A.; Yooseph, S.; Hall, A. P.; Liu, S.-Y.; Dorrestein, P. C.; Esquenazi, E.; Hunter, R. C.; Cheng, G.; et al. Cultivation of a human-associated TM7 phylotype reveals a reduced genome and epibiotic parasitic lifestyle. *Proc. Natl. Acad. Sci. U.S.A.* **2015**, *112* (1), 244–249.

(53) van Zyl, A. W.; Huddy, R.; Harrison, S. T. L.; van Hille, R. P. Evaluation of the ASTER^{TM} process in the presence of suspended solids. *Minerals Engineering*

2015, *76*, 72–80.
(54) Rahman, S. F.; Kantor, R. S.; Huddy, R. J.; Thomas, B. C.; van zyl, A. W.; Harrison, S. T. L.; Banfield, J. F. During mine water bioremediation, the presence of mineral particles decreases diversity and the abundance of *Thiobacilli* responsible for thiocyanate degradation. *MicrobiologyOpen*.
(55) Moraes, B. S.; Souza, T.; Foresti, E. Effect of sulfide concentration on autotrophic denitrification from nitrate and nitrite in vertical fixed-bed reactors. *Process Biochemistry* **2012**, No. 47, 1395–1401.
(56) Whitlock, J. L. Biological detoxification of precious metal processing wastewaters. *Geomicrobiology Journal* **1990**, *8* (3-4), 241–249.
(57) Stott, M. B.; Franzmann, P. D.; Zappia, L. R.; Watling, H. R.; Quan, L. P.; Clark, B. J.; Houchin, M. R.; Miller, P. C.; Williams, T. L. Thiocyanate removal from saline CIP process water by a rotating biological contactor, with reuse of the water for bioleaching. *Hydrometallurgy* **2001**, *62* (2), 93–105.
(58) Dictor, M. C.; Battaglia-Brunet, F.; Morin, D.; Bories, A.; Clarens, M. Biological treatment of gold ore cyanidation wastewater in fixed bed reactors. *Environ. Pollut.* **1997**, *97* (3), 287–294.
(59) Jeong, Y.-S.; Chung, J. S. Biodegradation of thiocyanate in biofilm reactor using fluidized-carriers. *Process Biochemistry* **2006**, *41* (3), 701–707.
(60) Ju, F.; Zhang, T. Experimental design and bioinformatics analysis for the application of metagenomics in environmental sciences and biotechnology. *Environ. Sci. Technol.* **2015**, *49* (21), 12628–12640.
(61) Roume, H.; Heintz-Buschart, A.; Muller, E. E. L.; May, P.; Satagopam, V. P.; Laczny, C. C.; Narayanasamy, S.; Lebrun, L. A.; Hoopmann, M. R.; Schupp, J. M.; et al. Comparative integrated omics: identification of key functionalities in microbial community-wide metabolic networks. *npj Biofilms and Microbiomes* **2015**, *1*, 15007.